Sensorless Control of Interior Permanent-Magnet Machine Drives With Zero-Phase Lag Position Estimation

Hyunbae Kim, *Student Member, IEEE*, Michael C. Harke, *Student Member, IEEE*, and Robert D. Lorenz, *Fellow, IEEE*

***Abstract*—This paper presents an improved method to estimate rotor motion states for an interior permanent-magnet machine drive. This approach is based on the estimation of a saliency-based electromotive force (EMF) in the stationary reference frame using a state filter. The spatial information obtained from the estimated saliency-based EMF is used in an observer to estimate the motor motion states. By using the commanded torque as a feedforward input to the observer, the motion state estimation has zero-phase lag, providing a very-high-bandwidth estimate.**

***Index Terms*—Interior permanent-magnet machine drive, observer-based control, sensorless control, state filter estimation.**

I. Introduction

WITHIN the last decade, significant improvements have been made in the area of sensorless control of permanent-magnet synchronous machines (PMSMs). The primary methods for sensorless position estimation can be divided into two main categories: approaches using back-electromotive-force (EMF) estimation with fundamental excitation [1]–[5] and spatial saliency image tracking methods using excitation in addition to the fundamental [5]–[10]. The saliency tracking methods are suitable for zero-speed operation, whereas the back-EMF-based methods fail at low speed.

Application of back-EMF-based methods to the symmetric PMSM is straightforward. However, when applying the methods to salient machines, such as the interior PMSM (IPMSM), necessary approximations lead to estimation errors and decreased performance. To solve this problem, a model was developed using a "saliency-based EMF" term in the stationary reference frame [2]. This saliency-based EMF consists of the salient terms of the machine model in addition to the EMF term. Application of the saliency-based EMF model was further improved by transformation to the rotor reference frame [3]. In [3], a state filter was used to estimate the saliency-based EMF, and an *arctan* function was used to estimate rotor position. Then, the rotor speed and position were estimated using a state filter with inherently lagging properties. Improvements to these methods can be realized with observer-based position and velocity estimation techniques using feedfoward torque command [14]. With the observer-based methods, torque accuracy is required to improve motion state estimation for dynamic trajectories.

For the IPMSM, inherent saliency, i.e., the difference between d-axis and q-axis inductance, beneficially changes both the air-gap torque production and the field weakening characteristics [11]. To take full advantage of these properties, the controller would ideally have accurate machine parameters. Maximum torque-per-amp control has been introduced to improve torque production in the constant torque region. The maximum torque-per-amp trajectory was calculated using fixed parameters. With this trajectory, the torque command is converted to i_{ds} and i_{qs} commands for a synchronous frame current regulator [11], [12]. A simple model based on measuring L_q, which depends on q-axis current, was developed to improve not only torque production but also torque accuracy [13]. Torque accuracy is achieved by a maximum torque-per-amp trajectory, including saturation [15].

This paper improves the saliency-based EMF methods by using an observer to estimate the motion states. By using the commanded torque from maximum torque-per-amp including saturation as feedforward into the observer, the lagging properties of the state filter can be eliminated. The result is zero-phase lag estimation of the motion states.

II. IPMSM Model in the Rotor Reference Frame

The model of the IPMSM in the rotor reference frame is outlined for the development of the position and velocity estimation method (1)

$$\begin{bmatrix} v_{ds}^r \\ v_{qs}^r \end{bmatrix} = \begin{bmatrix} r_s + pL_d & -\omega_r L_q \\ \omega_r L_d & r_s + pL_q \end{bmatrix} \begin{bmatrix} i_{ds}^r \\ i_{qs}^r \end{bmatrix} + \begin{bmatrix} 0 \\ \omega_r \lambda_{\rm pm} \end{bmatrix} \quad (1)$$

where

p	differential operator;
r_s	stator resistance;
L_d	total d-axis stator inductance $(= L_{md} + L_{ld})$;
L_q	total q-axis stator inductance $(= L_{mq} + L_{lq})$;
$\lambda_{\rm pm}$	permanent-magnet flux linkage;
i_{ds}^r	stator d-axis current in the rotor frame;
i_{qs}^r	stator q-axis current in the rotor frame;
v_{ds}^r	stator d-axis voltage in the rotor frame;
v_{qs}^r	stator q-axis voltage in the rotor frame.

Paper IPCSD 03–076, presented at the 2002 Industry Applications Society Annual Meeting, Pittsburgh, PA, October 13–18, and approved for publication in the IEEE TRANSACTIONS ON INDUSTRY APPLICATIONS by the Industrial Drives Committee of the IEEE Industry Applications Society. Manuscript submitted for review July 1, 2002 and released for publication July 7, 2003. This work was supported by the Wisconsin Electric Machines and Power Electronics Consortium (WEMPEC) of the University of Wisconsin, Madison, and by the National Science Foundation through the use of ERC Shared Facilities under Award EEC-9731677.

The authors are with the Department of Mechanical Engineering and Department of Electrical and Computer Engineering, University of Wisconsin, Madison, WI 53706 USA (e-mail: lorenz@engr.wisc.edu).

Digital Object Identifier 10.1109/TIA.2003.818966

0093-9994/03$17.00 © 2003 IEEE

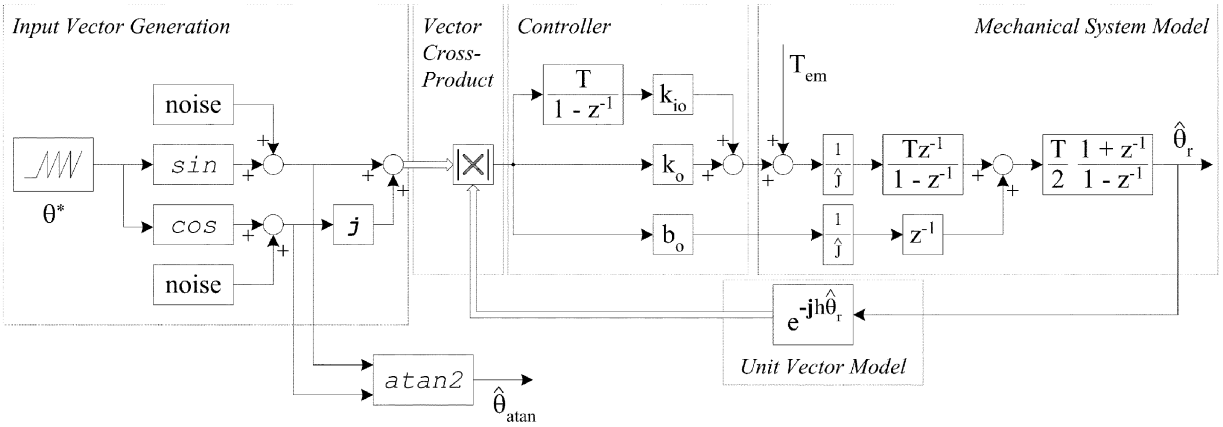

Fig. 1. Block diagram of the simulation comparing (a) observer-based, (b) state-filter-based, and (c) *arctan*-calculation-based position estimation.

In the application of standard back-EMF-based methods to IPMSM, transformation of the IPMSM model into an estimated rotor frame results in undesirable terms due to the saliency. In some methods of position estimation, the terms are ignored, resulting in performance degradation. In order to solve this problem, the IPMSM model can be rewritten to explicitly isolate the saliency-based EMF [2] in the rotor reference frame (2). The saliency-based EMF includes both the back-EMF $(\omega_r \lambda_{\rm pm})$ and the terms produced by the saliency in (3)

$$\begin{bmatrix} v_{ds}^s \\ v_{qs}^s \end{bmatrix} = \begin{bmatrix} r_s + pL_d & -\omega_r L_q \\ \omega_r L_q & r_s + pL_d \end{bmatrix} \begin{bmatrix} i_{ds}^s \\ i_{qs}^s \end{bmatrix} + \begin{bmatrix} 0 \\ E_{\rm sal} \end{bmatrix} \quad (2)$$

where

$$E_{\rm sal} = \omega_r \left[(L_d - L_q) i_{ds}^r + \lambda_{\rm pm} \right] - (L_d - L_q) p i_{qs}^r. \quad (3)$$

Equations (2) and (3) can be transformed into the stationary reference frame (4). The saliency-based EMF results in a rotating vector (5) and can be represented in complex vector form (6)

$$\begin{bmatrix} v_{ds}^s \\ v_{qs}^s \end{bmatrix} = \begin{bmatrix} r_s + pL_d & \omega_r (L_d - L_q) \\ -\omega_r (L_d - L_q) & r_s + pL_d \end{bmatrix} \times \begin{bmatrix} i_{ds}^s \\ i_{qs}^s \end{bmatrix} + \begin{bmatrix} E_{{\rm sal}\,ds}^s \\ E_{{\rm sal}\,qs}^s \end{bmatrix} \quad (4)$$

where

$$\begin{bmatrix} E_{{\rm sal}\,ds}^s \\ E_{{\rm sal}\,qs}^s \end{bmatrix} = E_{\rm sal} \begin{bmatrix} -\sin\theta_r \\ \cos\theta_r \end{bmatrix} \quad (5)$$

$$E_{{\rm sal}\,dqs}^s = E_{\rm sal} e^{j(\theta_r + \pi/2)}. \quad (6)$$

The saliency-based EMF (6) has spatial information in the vector angle that can be used for position estimation. The saliency-based EMF can exist at zero speed if i_{qs}^r varies: the second term of (3), $-(L_d - L_q) p i_{qs}^r$ exists at zero speed as the magnitude of the saliency-based EMF.

III. Zero-Phase Lag Position Estimation

Several methods can be used to estimate the position of a saliency-based rotating vector, including direct calculation using the *arctangent* of the two input signals [3], [10] and using a tracking observer [7]–[9]. The presence of noise on the measured signals results in noisy position estimates when using direct calculation methods such as the *arctan*. To reduce the noise problem, filters have been applied to either the estimated position or the input signals, adding lag to the estimate. By using an observer, noise on the position signals can be filtered without adding lag to the estimate.

To demonstrate the differences between the various topologies, a discrete-time simulation was performed. Fig. 1 is a block diagram of the simulation. Three position estimation methods were considered: tracking observer based, tracking state filter based, and *arctan* calculation based. The tracking state filter (or phase-locked loop) topology is similar to the observer except that it does not have the feedforward reference T_{em} and thus has inherently lagging estimation properties. The *Unit Vector Model* creates a rotating vector based on a harmonic h of the estimated position.

The eigenvalues of the tracking observer not only depend on the gains of the observer controller and the mechanical system model, but also on the magnitude of the input vector and the harmonic number of the saliency. Since the magnitude of the saliency-based EMF vector depends on the machine velocity, it must be decoupled from the input signal.

The *arctan* calculation has no intrinsic lag, but is sensitive to the signal-to-noise ratio. Advantages of the tracking observer include that it can track a signal with a much smaller signal-to-noise ratio than by using the *arctan*, it can be built in any reference frame, and can be used to track multiple saliencies [9]. The *arctan* calculation can only be used unambiguously on a single saliency.

In the simulation setup of Fig. 1, a commanded position trajectory is used to calculate a rotating unit vector. A random noise limited to 10% of the vector magnitude is added to the unit vector. This sum is used to test the dynamic tracking of the three position estimation methods.

The position estimation of the *arctan* direct calculation has no lag, but suffers from a large position estimate error due to the noise, Fig. 2. The effect of the noise can be mitigated using a state filter, but the estimate then has lagging properties, Fig. 3. Similar results occur when applying a low-pass filter to the direct calculation method. By using an observer topology with the appropriate feedforward command, zero lag properties can be

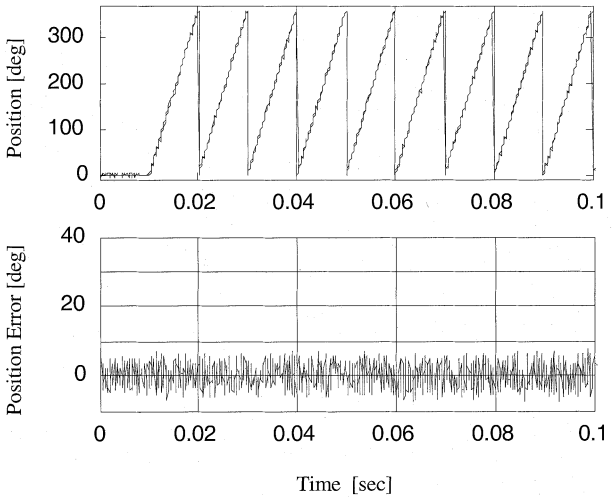

Fig. 2. Simulated position, estimated position, and position error for an *arctan* position estimator.

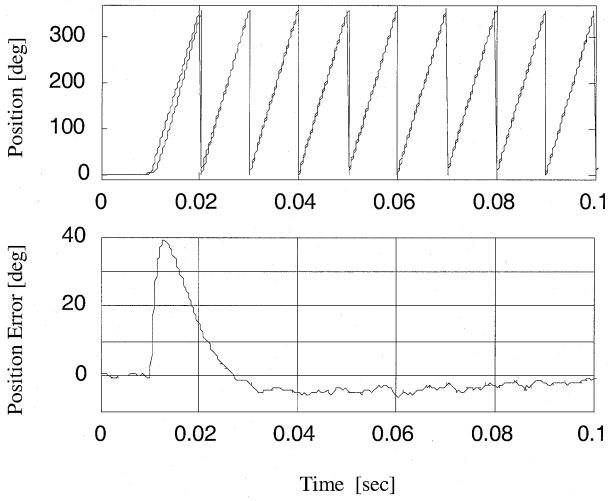

Fig. 3. Simulated position, estimated position, and position error for a tracking state filter position estimator (eigenvalues: 5000, 110, 20, and 4 Hz).

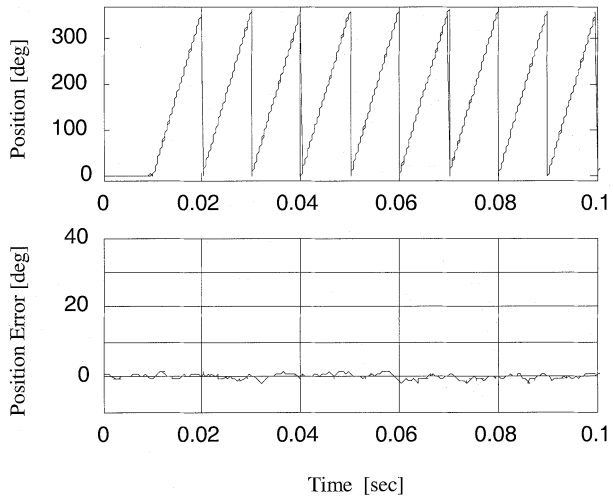

Fig. 4. Simulated position, estimated position, and position error for a tracking observer position estimator (eigenvalues: 5000, 110, 20, and 4 Hz).

achieved, Fig. 4. It is also possible to construct the state observer topology using the *arctan* to generate the observer reference. This produces similar results to the vector-tracking observer, but requires use of the *arctan* function.

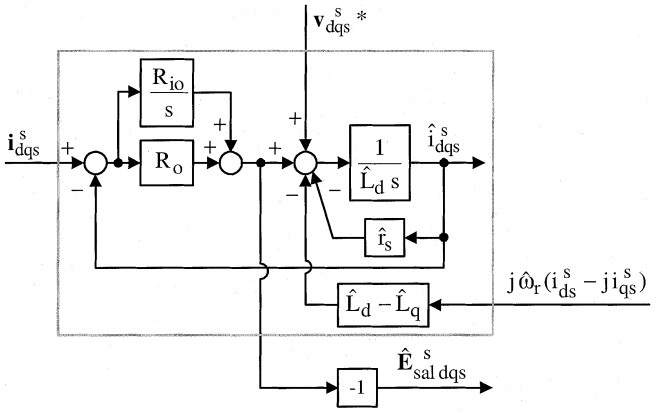

Fig. 5. Proposed state filter for estimation of the saliency-based EMF within the state filter bandwidth.

IV. Estimation Method

A. State Filter for Estimation of the Saliency-Based EMF in the Stationary Reference Frame

The saliency-based EMF can be estimated using a state filter, Fig. 5, based on a current observer. The state filter consists of two parts: the IPMSM model without the saliency-based EMF terms (6) and a proportional–integral (PI) compensator. Since the saliency-based EMF is unmodeled, it is inherently estimated by the PI compensator. However, the estimation bandwidth is limited by the state filter bandwidth and inherently has lagging properties.

The estimation of the saliency-based EMF from the proposed state filter is represented by (7)

$$\begin{aligned}\hat{\boldsymbol{E}}^{s}_{\text{sal } dqs} =& \frac{R_o s + R_{io}}{\hat{L}_d s^2 + (\hat{r}_s + R_0)s + R_{io}} \boldsymbol{E}^{s}_{\text{sal } dqs} \\ &+ \frac{R_o s + R_{io}}{\hat{L}_d s^2 + (\hat{r}_s + R_o)s + R_{io}} \\ &\times \Big\{ \boldsymbol{v}^{s^*}_{dqs} - v^2_{dqs} + (L_d - \hat{L}_d) s \boldsymbol{i}^{s}_{dqs} \\ &\quad + (r_s - \hat{r}_s)\boldsymbol{i}^{s}_{dqs} \\ &\quad + [(L_d - L_q) j\omega_r - (\hat{L}_d - \hat{L}_q) j\hat{\omega}_r] \\ &\quad \times \left(i^s_{ds} - i^s_{qs}\right) \Big\}. \end{aligned} \tag{7}$$

The estimation accuracy of the saliency-based EMF state filter is determined by the bandwidth of the state filter and the errors in parameter estimation and reference voltage. Fig. 6 is a plot of the theoretical estimation accuracy frequency response function (FRF) for the saliency-based EMF state filter assuming no parameter estimation and reference voltage errors. The closed-loop eigenvalues are set at 200 and 250 Hz. Phase lag can be seen above the bandwidth of the state filter, Fig. 6. The bandwidth of the state filter is limited by undesirable harmonics due to inverter nonlinearities and secondary machine harmonics.

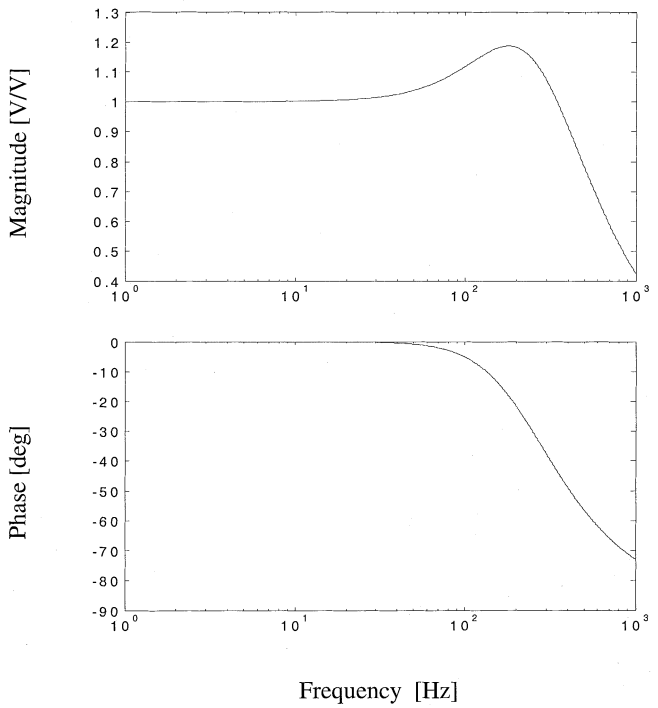

Fig. 6. Estimation accuracy FRF for the saliency-based EMF state filter with eigenvalues set to 200 and 250 Hz.

For high-speed applications, care must be taken when implementing the saliency-based EMF state filter in the digital domain. Because the state filter uses the commanded voltages for feedforward and the measured currents as the state reference, the timing delays in the controller and inverter should be included in the model. This can be accomplished by using the modified z-transform [16].

B. Saliency Tracking Observer for Estimation of Position and Velocity With Zero-Phase Lag

The estimated saliency-based EMF from the state filter, Fig. 5, contains rotor position information (8)

$$\hat{\boldsymbol{E}}^{s}_{\text{sal}\ dqs} = \hat{E}_{\text{sal}} e^{j(\theta_r+\pi/2)} = \begin{bmatrix} \hat{E}^{s}_{\text{sal}\ ds} \\ \hat{E}^{s}_{\text{sal}\ qs} \end{bmatrix} = \hat{E}_{\text{sal}} \begin{bmatrix} -\sin\theta_r \\ \cos\theta_r \end{bmatrix}. \tag{8}$$

If the *arctan* function method is used, then the electrical rotor position is directly estimated by using (9)

$$\hat{\theta}_r = \tan^{-1} - \frac{\hat{E}^{s}_{\text{sal}\ ds}}{\hat{E}^{s}_{\text{sal}\ qs}}. \tag{9}$$

Either a vector tracking observer or state filter (based on phase-locked loop methods) can be used to estimate the motion states from the estimated saliency-based EMF without using the *arctan* function. The phase error between the estimated saliency-based EMF (from the previous state filter) and the saliency-based EMF model is fed in to the observer controller, Fig. 7.

A vector cross product is one method of detecting the phase error between between the estimated saliency-based EMF and a saliency-based EMF model. This results in an error term that only has a single phase error component (10)

$$\varepsilon = |\hat{E}_{\text{sal}}| \sin(\theta_r - \hat{\theta}_r). \tag{10}$$

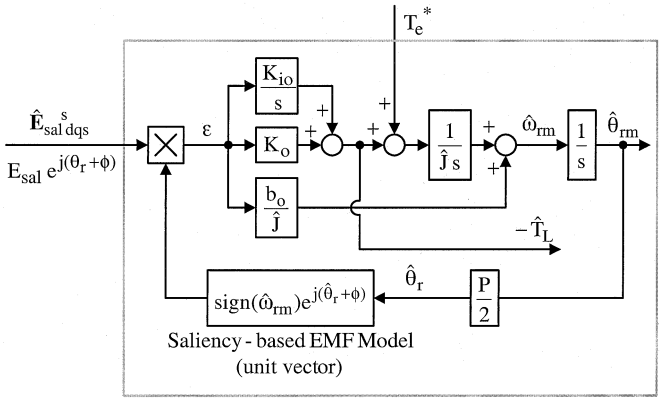

Fig. 7. Proposed observer in cascade with the state filter of Fig. 5 for tracking the angle of the saliency-based EMF.

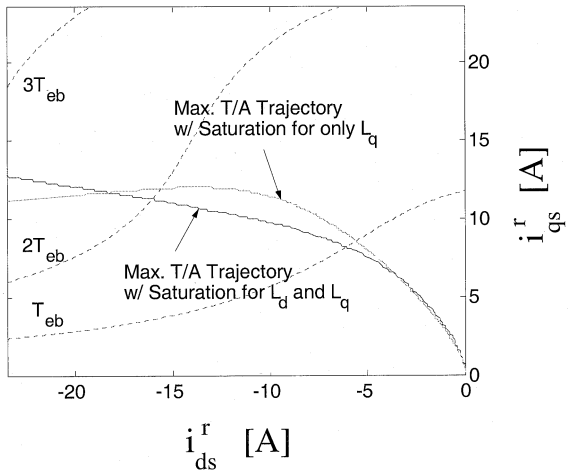

Fig. 8. Constant torque loci and maximum torque-per-amp trajectory including saturation assuming fixed parameters.

The physical system model consists of a second-order system with one parameter, the estimated inertia. The error between torque command and actual torque depends on current regulator bandwidth and estimated parameter accuracy in the calculation of maximum torque-per-amp trajectory which is converted to d-axis and q-axis current. Since parameters (including L_d and L_q) change with operating conditions due to magnetic saturation, continuously estimated parameters should be used for the calculation [15]. By using the continuously estimated parameters, the error between the commanded torque and actual torque is reduced. Cross saturation will cause some small errors in the estimated parameters during transient operation.

Fig. 8 shows the maximum torque-per-amp trajectory considering magnetic saturation, derived from experimental data. The maximum torque-per-amp is a function of L_d, L_q and λ_{pm}. With this calculation, λ_{pm} is assumed to be constant. L_d and L_q change nonlinearly with increasing current. Therefore, the trajectory of Fig. 8 is calculated by using fixed nominal values and adjusting the current commands to produce a

maximum torque-per-amp trajectory. The actual maximum torque-per-amp trajectory including magnetic saturation could also be calculated by using the measured parameters as they vary with operating conditions. If an off-line parameter estimation method is used to obtain parameters for a range of operating conditions, this trajectory can be calculated. However, this is computationally intensive due to the nonlinearity of the saturation. Such calculations are usually unreasonable in real time unless simple online parameter estimation methods are employed [15].

With a high-bandwidth current regulator, the estimated electromagnetic torque command for the observer can be expressed as follows:

$$T_e^* = \hat{T}_e = \frac{3}{4} P \left[\hat{\lambda}_{\rm pm} i_{qs}^r + (\hat{L}_d - \hat{L}_q) i_{qs}^r i_{ds}^r \right] \qquad (11)$$

where P is the number of poles.

The velocity and position estimation transfer functions are represented by (12) or (13) using (11) and assuming $\hat{\lambda}_{\rm pm} = \lambda_{\rm pm}$ or $\hat{L}_d - \hat{L}_q = L_d - L_q$, respectively,

$$\frac{\hat{\omega}}{\omega} = \frac{\hat{\theta}}{\theta} = \frac{J \frac{\hat{L}_d - \hat{L}_q}{L_d - L_q} s^3 + b_o s^2 + K_o s + K_{io}}{\hat{J} s^3 + b_o s^2 + K_o s + K_{io}} \qquad (12)$$

or

$$\frac{\hat{\omega}}{\omega} = \frac{\hat{\theta}}{\theta} = \frac{J \frac{\hat{\lambda}_{\rm pm}}{\lambda_{\rm pm}} s^3 + b_o s^2 + K_o s + K_{io}}{\hat{J} s^3 + b_o s^2 + K_o s + K_{io}}. \qquad (13)$$

The error between commanded torque and actual torque is a function of parameter errors (L_d, L_q and $\lambda_{\rm pm}$). While the torque error results in velocity estimation error, it can be mitigated using a maximum torque-per-amp trajectory that includes magnetic saturation.

Fig. 9 is a plot of the theoretical estimation accuracy frequency response for the saliency tracking observer. The closed-loop eigenvalues are set at 500, 100, and 20 Hz. The observer (and previous state filter) must have adequate bandwidth in order to maintain adequate dynamic stiffness (disturbance rejection) in the motion controller.

The observer is insensitive to mechanical parameter estimation error and torque error within the bandwidth of the observer. These errors will result in position estimation error at frequencies above the observer bandwidth.

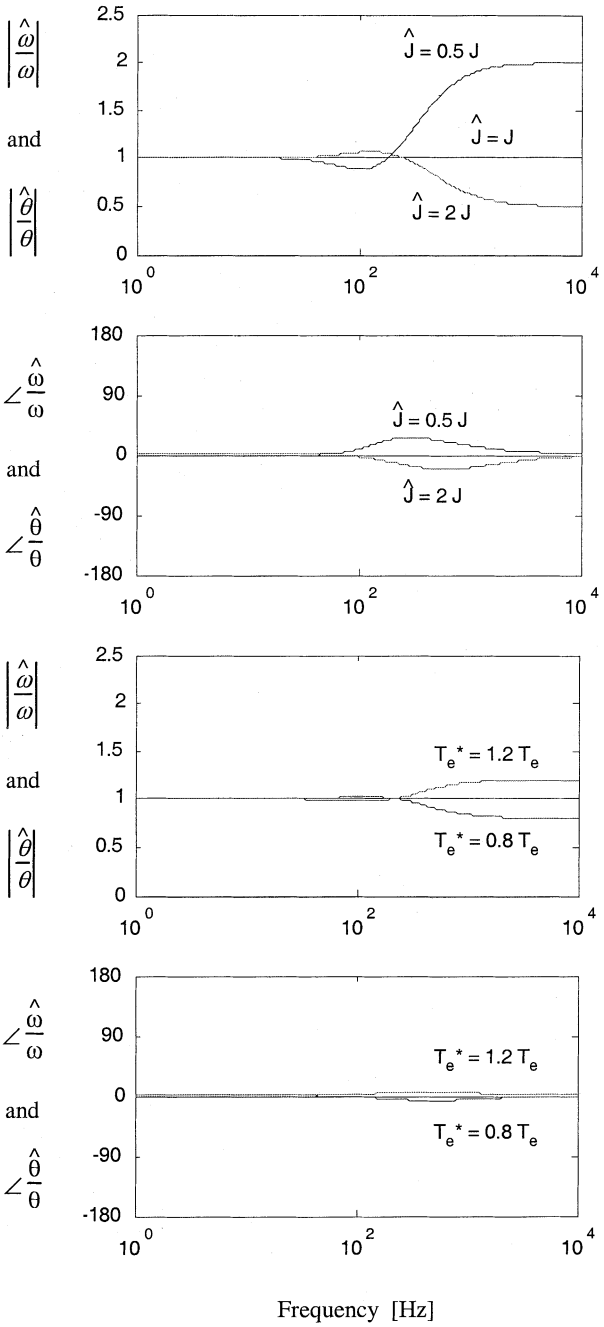

Fig. 9. Estimation accuracy frequency response for the saliency tracking observer showing $\hat{J}$ and $\hat{T}_e$ parameter insensitivity.

V. Sensorless Torque Control

Fig. 10 shows a block diagram of the IPMSM controller including position estimation and the maximum torque-per-amp trajectory tables. The current commands are based on a maximum torque-per-amp trajectory which includes saturation [15].

VI. Experimental Results

The saliency-based EMF position estimation method was tested on a DSP controlled IPMSM coupled to a load motor, Fig. 11. The switching and sampling rate of the hardware system is 8 kHz. Nominal parameters for the test motor are provided in Table I.

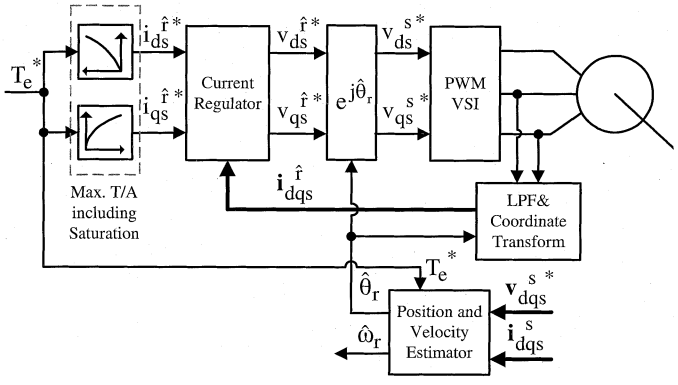

Fig. 10. Block diagram of the proposed IPMSM controller including sensorless position estimation and maximum torque-per-amp trajectory tables.

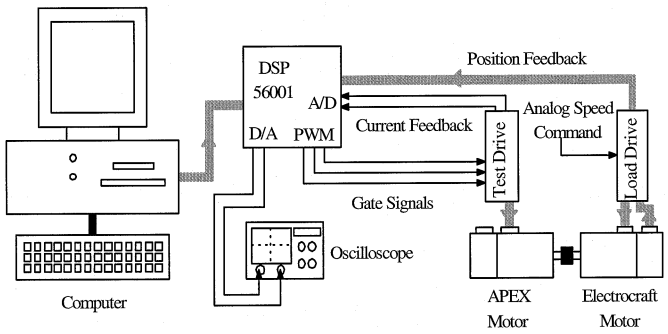

Fig. 11. Experimental test setup.

TABLE I
IPMSM NOMINAL PARAMETERS

Parameter	Value
Max. Torque	7.7 N·m
Max. Speed	6200 rpm
r_s	1.5 Ω
L_q	11 mH
L_d	3.7 mH
λ_{pm}	0.086 Wb
J	1.0 kg·m^2×10^{-4}
Poles	4

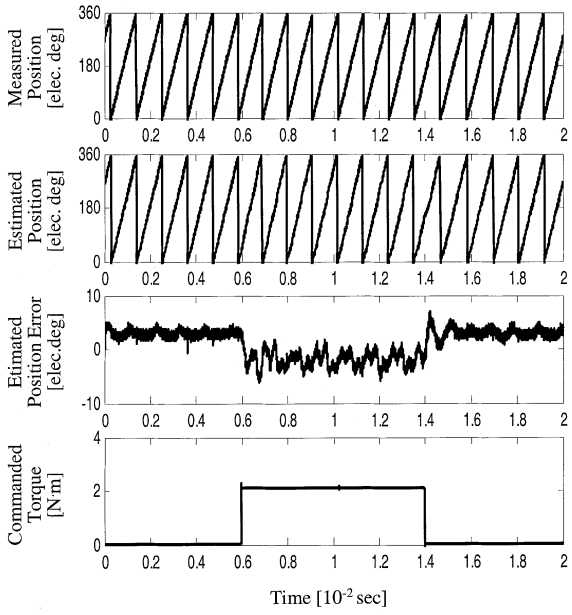

Fig. 12. Estimated torque load change at rotor speed = 2700 r/min.

Fig. 12 is a plot of the estimated and measured electrical rotor position with a step change to rated torque while the motor is running at constant speed (2700 r/min). Position estimation is robust under the transient step torque change, due to the feedforward torque command path to the observer. The magnitude of saliency-based EMF is determined by operating conditions (ω_r, i^r_{ds}, pi^r_{qs}) and parameters (L_d, L_q, $\lambda_{\rm pm}$) in (3). Since the back-EMF term $(\omega_r\lambda_{\rm pm})$ is relatively dominant at high speeds in the saliency-based EMF (3), the change in magnitude due to the change in load is relatively small. The state filter in Fig. 5

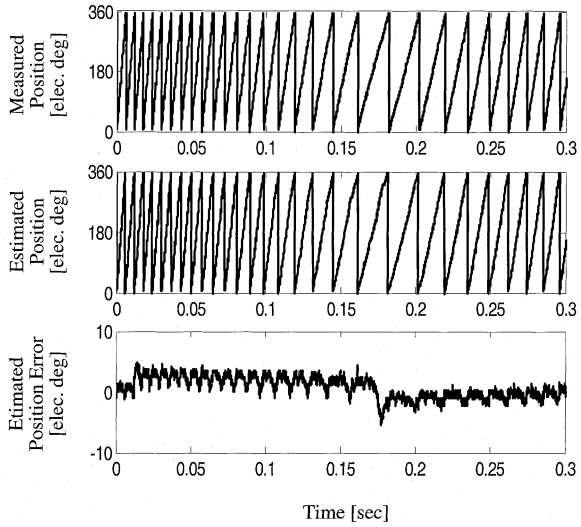

Fig. 13. Estimated and measured electrical rotor position with varying speed (1000–5000 r/min) at half rated load.

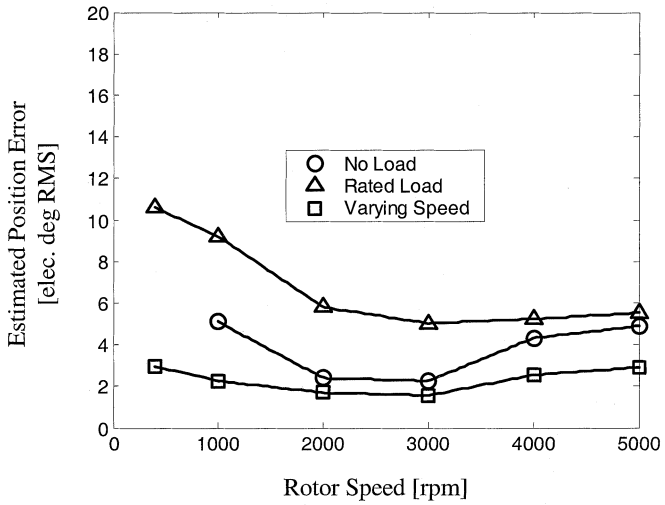

Fig. 14. Estimated position error versus motor speed at rated and no load with constant speed, and at half rated load with varying speed (±300 r/min).

extracts the saliency-based EMF, filtering out higher frequency harmonics. Therefore, the observer of Fig. 7 properly tracks the estimated saliency-based at high speeds under a step rated load change.

Fig. 13 is plot of the estimated and measured electrical position with varying motor speed at half rated load. This demonstrates that phase-lag is kept to a minimum during a transient command due to the feedforward input of the observer. The proposed speed estimation algorithm is also suitable over a wide speed range.

Fig. 14 is a plot of the estimated position error versus rotor speed at rated load and no load with constant speed, and at half-rated load with varying speed (operating speed ±300 r/min). Due to computational limitations in the test setup, parameter estimation could not be implemented concurrently with the saliency-based EMF tracking techniques. The resulting inductance parameter estimation errors affect the position accuracy at low speeds when the back-EMF is small. In addition, at low speed and voltage the saliency-based EMF state filter is sensitive to the

stator resistance estimation. Other sources of error that affect the accuracy at low speeds include inverter harmonics and secondary machine harmonics. If these harmonics are within the bandwidth of the state filter, they will lead to position estimation errors. At higher speeds, the position estimation errors result from the bandwidth limitations of the saliency-based EMF state filter. The state filter bandwidth is limited by the quantization noise and inverter nonlinearities.

The position estimation errors decrease the torque production of the machine. The sensitivity of the torque production to position estimation errors depends on the machine design and the amount of reluctance torque for the machine.

With varying speed, the effect of the torque feedforward path to the tracking observer reduces the amount of position error. The primary function of the torque feedforward in the tracking observer is to handle the dynamic torque command trajectories of the machine.

VII. Conclusion

This paper has presented an improved method of estimating the rotor position using a saliency-based EMF. A state filter is used to estimate the saliency-based EMF. In cascade, a tracking observer is used to estimate the rotor position. While the tracking observer topology does not introduce phase lag to the estimate, the state filter does. This is a limitation of the proposed method. The following points summarize the work presented.

- An IPMSM model in the stationary reference frame with a saliency-based EMF is used for position estimation.
- A state filter is developed for saliency-based EMF estimation and a tracking observer is developed, including the mechanical model for position estimation.
- Direct *arctan* calculation-based methods for position estimation are sensitive to signal noise. Filtering reduces the problem caused by the input signal noise, but adds phase lag to the estimate. By properly forming an observer, a filtered position estimate with zero-phase lag is realized.
- Nearly zero-phase lag estimation for rotor position and velocity can be achieved using a cascaded observer with a feedforward torque command. This allows substantially improved dynamic response of the IPMSM motion controller.
- Maximum torque-per-amp trajectory, including iron saturation, was used to improve the torque control accuracy. This reduces the error between torque command and actual airgap torque, minimizing errors in the motion state observer.

References

[1] R. Wu and G. Slemon, "A permanent magnet motor drive without a shaft sensor," *IEEE Trans. Ind. Applicat.*, vol. 27, pp. 1005–1011, Sept./Oct. 1991.

[2] Z. Chen, M. Tomita, S. Ichikawa, S. Doki, and S. Okuma, "Sensorless control of interior permanent magnet synchronous motor by estimation of an extended electromotive force," in *Conf. Rec. IEEE-IAS Annu. Meeting*, vol. 3, Rome, Italy, Oct. 2000, pp. 1814–1819.

[3] S. Morimoto, K. Kawamoto, M. Sanada, and Y. Takeda, "Sensorless control strategy for salient-pole PMSM based on extended EMF in rotating reference frame," *IEEE Trans. Ind. Applicat.*, vol. 38, pp. 1054–1061, July/Aug. 2002.

[4] K. Sakamoto, Y. Iwaji, T. Endo, and Y. Takakura, "Position and speed sensorless control for PMSM drive using direct position error estimation," in *Proc. IEEE IECON'01*, vol. 3, 2001, pp. 1680–1685.

[5] N. Patel, T. O'Meara, J. Nagashima, and R. D. Lorenz, "Encoderless IPM traction drive for EV/HEV's," in *Conf. Rec. IEEE-IAS Annu. Meeting*, vol. 3, Chicago, IL, Sept. 30–Oct. 5, 2001, pp. 1703–1707.

[6] S. Ogasawara and H. Akagi, "Implementation and position control performance of a position-sensorless IPM motor drive system based on magnetic saliency," *IEEE Trans. Ind. Applicat.*, vol. 34, pp. 806–812, July/Aug. 1998.

[7] M. Corley and R. Lorenz, "Rotor position and velocity estimation for salient-pole permanent magnet synchronous machine at standstill and high speed," *IEEE Trans. Ind. Applicat.*, vol. 34, pp. 784–789, July/Aug. 1998.

[8] P. L. Jansen and R. D. Lorenz, "Transducerless position and velocity estimation in induction and salient AC machines," *IEEE Trans. Ind. Applicat.*, vol. 31, pp. 240–247, Mar./Apr. 1995.

[9] M. W. Degner and R. D. Lorenz, "Using multiple saliencies for the estimation of flux, position, and velocity in AC machines," *IEEE Trans. Ind. Applicat.*, vol. 34, pp. 1097–1104, Sept./Oct. 1998.

[10] N. Teske, G. M. Asher, M. Sumner, and K. J. Bradley, "Analysis and suppression of high-frequency inverter modulation in sensorless position-controlled induction machine drives," *IEEE Trans. Ind. Applicat.*, vol. 39, pp. 10–18, Jan./Feb. 2003.

[11] T. M. Jahns, G. B. Kliman, and T. W. Neumann, "Interior permanent-magnet synchronous motors for adjustable-speed drives," *IEEE Trans. Ind. Applicat.*, vol. 22, pp. 738–747, July/Aug. 1986.

[12] S. R. MacMinn and T. M. Jahns, "Control techniques for improved high-speed performance of interior PM synchronous motors drives," *IEEE Trans. Ind. Applicat.*, vol. 27, pp. 997–1004, Sept./Oct. 1991.

[13] S. Morimoto, T. Ueno, M. Sanada, and A. Yamagiwa, "Effects and compensation of magnetic saturation in permanent magnet synchronous motor drives," in *Conf. Rec. IEEE-IAS Annu. Meeting*, vol. 1, Oct. 1993, pp. 59–64.

[14] R. D. Lorenz, "Microprocessor control of motor drives and power converters—Microprocessor motion control of AC and DC drives," in *IEEE Tutorial Course Notebook from 1991, 1992, and 1993 IEEE-IAS Annual Meetings.* Piscataway, NJ: IEEE Press, 1991–1993, ch. 4.

[15] H. Kim, J. Hartwig, and R. D. Lorenz, "Using on-line parameter estimation to improve efficiency of IPM machine drives," in *Proc. IEEE PESC*, vol. 2, June 2002, pp. 815–820.

[16] K. Ogata, *Discrete-Time Control Systems*, 2nd ed. Upper Saddle River, NJ: Prentice-Hall, 1995.

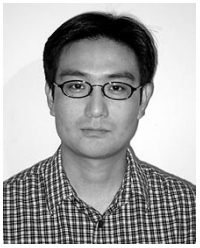

Hyunbae Kim (S'01) received the B.S. degree in 1996 from Kunsan National University, Kunsan, Korea, and the M.S. degree in mechanical engineering in 1999 from the University of Wisconsin, Madison, where he is currently working toward the Ph.D. degree in mechanical engineering.

His research interest is high-performance permanent-magnet machine drives including self-sensing.

Michael C. Harke (S'98) received the B.S. and M.S. degrees in mechanical engineering in 1997 and 1999, respectively, from the University of Wisconsin, Madison, where he is currently working toward the Ph.D. degree in mechanical engineering.

The focus of his research is on sensorless control of permanent-magnet machines. His research interests include control systems, electric machines, power electronics, and machine design.

Robert D. Lorenz (S'83–M'84–SM'91–F'98) received the B.S., M.S., and Ph.D. degrees from the University of Wisconsin, Madison, and the M.B.A. degree from the University of Rochester, Rochester, NY.

Since 1984, he has been a member of the faculty of the University of Wisconsin, Madison, where he is the Mead Witter Foundation Consolidated Papers Professor of Controls Engineering in both the Department of Mechanical Engineering and the Department of Electrical and Computer Engineering. He is Co-Director of the Wisconsin Electric Machines and Power Electronics Consortium, which celebrated its 20th anniversary in 2001. It is the largest industrial research consortium on motor drives in the world. He is also the thrust leader for control and sensor integration in the Center for Power Electronic Systems, an NSF Engineering Research Center (ERC) which is a joint ERC with Virgina Polytechnic Institute and State University, Rensselaer Polytechnic Institute, University of Puerto Rico-Mayaguez, and North Carolina A&T. From 1972 to 1982, he was a member of the research staff at the Gleason Works, Rochester, NY, working principally on high-performance drives and synchronized motion control. He was a Visiting Research Professor in the Electrical Drives Group, Catholic University of Leuven, Leuven, Belgium, in the summer of 1989 and in the Power Electronics and Electrical Drives Institute, Technical University of Aachen, Aachen, Germany, in the summers of 1987, 1991, 1995, 1997, and 1999, where he also was the SEW Eurodrive Guest Professor from September 1, 2000 until July 7, 2001. In 1969–1970, he conducted Master thesis research in adaptive control of machine tools at the Technical University of Aachen. His current research interests include sensorless electromagnetic motor/actuator technologies, real-time signal processing and estimation techniques, precision multiaxis motion control, and ac/dc drive and high-precision machine control technologies. He has authored more than 160 published technical papers and is the holder of 16 patents, with two more pending.

Dr. Lorenz was the IEEE Industry Applications Society (IAS) President for 2001, a Distinguished Lecturer of the IAS for 2000/2001, immediate past Chair of the IAS Awards Department, and past Chairman of the IAS Industrial Drives Committee, and is a member of the IAS Industrial Drives, Electric Machines, Industrial Power Converter, and Industrial Automation and Control Committees. He is also the current Chair of the Periodicals Committee for the IEEE Technical Activities Board. He is a member of the IEEE Sensor Council AdCom. He is a Registered Professional Engineer in the States of New York and Wisconsin. He is also a member of the American Society of Mechanical Engineers, Instrument Society of America, and Society of Photo-Optical Instrumentation Engineers. He has won 15 prize paper awards.